Numerical and Experimental Determination of Strains in the Vicinity of a Centrally Located Circular Discontinuity in AA6061-T6 Square Extrusions during Axial Crushing

Neil Turton, Amitabha Majumder, William Altenhof, Daniel Green, Vivek Vijayan, Honggang An, and Shun Yi Jin

Department of Mechanical, Automotive and Materials Engineering,
University of Windsor, 410 Sunset Avenue, Windsor, N9B 3P4, Ontario, Canada

Abstract

An experimental and numerical investigation was conducted on AA6061-T6 extrusions with centrally located through-hole discontinuities to investigate the strains in the vicinity of the crush trigger. The extrusions used in this research were of square cross sectional geometry with a nominal side width of 38.1 mm, wall thickness of 3.15 mm and length of 200 mm. Centrally located circular discontinuities with a diameter of 14.29 mm were incorporated into the extrusion through CNC machining. The axial crushing tests were performed in a quasi-static manner using a hydraulic Tinius-Olsen tension/compression testing machine and observed using a GOM Aramis optical strain measuring device focusing on the region in the vicinity of the discontinuity. A finite element model previously developed by Arnold and Altenhof was selected to compare strains in the region of the through-hole. The material definition for the AA6061-T6 extrusion utilized in this FE model incorporated damage mechanics theory which was able to accurately predict material failure after a two-stage calibration process. All simulations considered in this research were completed using LS-DYNA® version 970 revision 5434a. Good predictive capabilities of the strain magnitudes and distributions were observed from the numerical simulations. In the vicinity of the discontinuity, at the stress concentration region and at maximum crushing force, the effective strain was observed to range from 4.5% to 15.5% in LS-DYNA simulations. Experimental observations on the effective strain ranged from 5.0% to 15.7%. This information is important in the understanding of large deformation behaviour for AA6061-T6 extrusions, which could be applied in structural crashworthiness applications.

Introduction

Structural members with circular discontinuities are widely used in automotive chassis and other applications as energy dissipation mechanisms. However, the development of the strain concentration, in elastic-plastic deformation, near the discontinuity has not been extensively investigated.

Jones and Abramowicz [1] experimentally and analytically investigated square and circular cross sectional metal extrusions as energy absorbing structures under axial quasi-static and dynamic loading conditions. Abramowicz and Jones [2] further extended their work on the investigation of influence of extrusion geometry parameters on the deformation modes, namely, progressive folding, global bending and transition of global bending and progressive folding.

Crush initiators, including material and geometrical variations, can be used as control methods to avoid unfavorable deformation resulting from global bending or other catastrophic modes under compressive loading. Introducing a geometrical discontinuity to a structural member can initiate a specific collapse mode in the axial direction, minimize the peak crush load, and improve the crush force efficiency.

Krauss and Laananen [3] studied the presence of circular and diamond shaped holes, and cross-sectional beads in square steel tubes subjected to dynamic axial loading with a reduction of maximum crush loads of approximately 40% reported. Abah et al. [4] investigated different sizes of circular discontinuities in axially loaded aluminum square extrusions. These crush triggers caused a decrease in peak crush load proportional to the increase in the size of the discontinuity. In this research it was observed that the mean crush load remained relatively constant for all trigger geometries considered.

Arnold and Altenhof [5] experimentally studied the quasi-static axial compression of square AA6061-T4 and-T6 tubes with the presence of circular discontinuities. A significantly lower peak crush load and higher crush force efficiency were reported on the extrusions with circular discontinuities. With the presence of a centrally located circular discontinuity in the extrusion, the energy absorption capacity had been greatly improved through altering of the deformation mode.

In recent years, digital image correlation (DIC) has been introduced to study two- and three-dimensional full-field strain distributions using photogrammetry technology. Photogrammetry is an optical method, utilizing an arranged or random grid, which determines the three-dimensional coordinate data on the surface of an object. The system uses triangulation to determine precise location of all pixel coordinates in images from two cameras, and calculates the three dimensional coordinates to obtain the precise shape of the object.

DIC has successfully been applied in a variety of applications. For example, Tyson et al. [6] used the full-field optical measuring technique for measurement of strain variations in biological tissues. Additionally, Tyson et al. [7] have also applied this technique for strain determinations in a variety of challenging environments. Jin [8] conducted three separate types of compression experiments on foam specimens and demonstrated that the DIC technique is able to obtain accurate and full-field large deformation strain measurement of foam specimens. The experiments conducted by Jin also presented the influence of loading configurations on deformation and strain concentration in foam specimens.

This research focuses on the development of a numerical model to study the effect of strain concentrations, in the vicinity of a centrally located circular discontinuity, on deformation mode. Model validation is achieved through a direct comparison of experimental observations utilizing the DIC technique. In this investigation the ARAMIS optical strain measurement system was used.

Experimental Procedure

Tensile Testing of Extrusion Material AA6061-T6

In order to obtain material properties of the AA6061-T6 aluminum extrusions, eight tensile tests were performed in accordance to ASTM standard E8M [9] on an INSTRON 8562 tensile testing machine with a 100kN load capacity. Prior to tensile testing, surface treatment of the specimens, for optical strain measurement, was completed by first cleaning the specimens with a diluted acetone mixture. After drying a thin coating of white paint was applied and allowed to dry. A black speckled pattern was applied onto the white surface for high contrast. The speckles were

carefully applied onto the surface such that the average diameter measured approximately 3 to 5 pixels within the field of view.

For the tensile testing, the field of view was selected as 65 mm by 52 mm. Additionally, an extensometer with a gauge length of 25.4 mm was applied to the reduced region of the tensile specimen prior to testing. Data sampling rates for the INSTRON (load cell and extensometer) and ARAMIS systems were 40 Hz and 0.5 Hz respectively. The displacement rate for the translating crosshead of the testing machine was 5 mm/min.

In order to validate the ARAMIS data, strains at five locations within the gauge region were compared to the strains obtained from the extensometer. Figure 1a illustrates the strain for a representative specimen, in the loading direction, as a function of time for the five locations (as measured from the ARAMIS system) and extensometer. As evident in Figure 1a, good agreement between strain measurements from the ARAMIS system and extensometer were observed. Deviation between both measuring techniques is observed at approximately 280 s as a result of necking in the tensile specimen.

For the eight tensile tests completed appropriate repeatability was observed. For clarity a single representative stress/strain profile for the AA6061-T6 material is presented in Figure 1b.

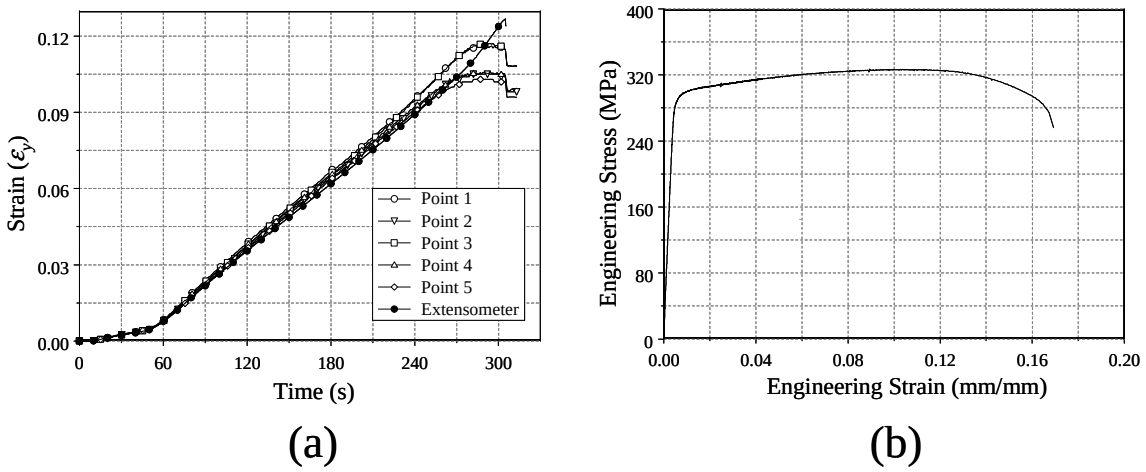

Figure 1. (a) Strain/time profiles from extensometer and ARAMIS system. (b) Engineering stress/strain response of AA6061-T6 sidewall material.

Extrusion Geometry and Experimental Quasi-static Axial Crushing Method

The aluminum extrusions used in this research were square cross section AA6061-T6 tubes with a nominal side width (C) of 38.1 mm, wall thickness (t) of 3.15mm and length (L) of 200 mm. Under compressive axial loading, the structures, without any circular discontinuity, had L/C and C/t ratios that resulted in a prediction of global bending according to theoretical and empirical predictions reported by Abramowicz and Jones [2]. Circular holes with diameters of 14.29mm were selected as the geometrical discontinuities to be investigated in this research. Specimens with circular holes were fabricated using a CNC milling machine. No de-burring treatment was needed by application of the machining methods. Extrusion specimen preparation was completed

following the identical procedure previously detailed for the tensile specimens. Paint application was completed on one side wall of the extrusion containing the discontinuity.

Compressive tests were completed on a hydraulic Tinius–Olsen testing machine. Specimens were placed on the centre of a translating crosshead such that the axial direction of the test specimen was parallel to the direction of motion of the moving crosshead. A fixed crosshead was located above the test specimen. Testing data were collected using the ARAMIS optical measurement device at a rate of 0.5 Hz. A computer equipped with the ARAMIS analysis software was used to record the measurements from the cameras and the load cell and linear voltage differential transformer (LVDT), the later two devices being incorporated into the testing machine. The specimens were crushed at a nominal crosshead speed of 15 mm/min. Five experimental tests, completed at room temperature, were conducted on extrusions having the discontinuity.

Numerical Model Development

A finite element (FE) model was developed to simulate the quasi-static crush tests for the AA6061-T6 specimen with the circular hole discontinuity.

Discretization of the specimen models

Discretization of the extrusion with the 14.29 mm discontinuity was carried out using the parametric mesh generation software TrueGrid. Figure 2 illustrates the mesh density in the extrusion. Due to the symmetry observed in all the experimental quasi-static crushing tests, only half of the extrusion geometry was developed. Mesh size and quality was based upon details of a

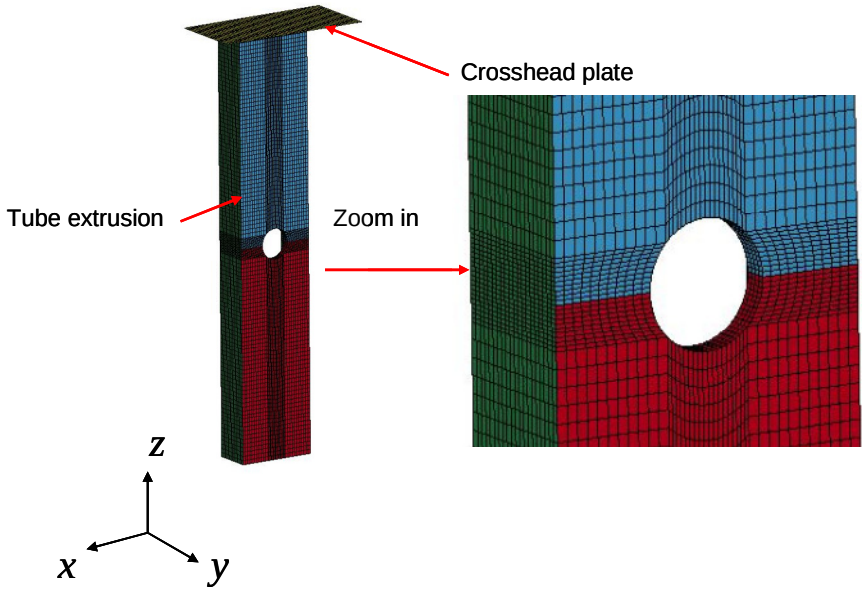

Figure 2. Discretization of the extrusion.

finite element model developed and validated by Arnold [10] investigating the load/displacement characteristics of the identical extrusion. To appropriately model material failure, a fine discretization was used in the vicinity of the discontinuity (as illustrated in Figure 2). Furthermore, in order to accurately capture the stress distribution through the extrusion wall

thickness, four elements were utilized through the thickness of the tube. Selectively reduced hexahedral brick elements were used as the element formulation of the extrusion. The main advantage of using this element is to eliminate the zero energy modes of deformation.

Shell elements employing a rigid material definition were used to model the crosshead of the compressive testing machine, as shown in Figure 2. The mesh density used for these shell elements was consistent to that of the extrusion model.

Modeling contact

Contact was modeled between the rigid plate and the extrusion using a surface-to-surface contact algorithm available in LS-DYNA®. Due to the nature of the collapse mode observed in the experimental testing, it was necessary to model contact between the walls of the tube. This was implemented using a single-surface contact algorithm available in LS-DYNA. Both contact algorithms used in the models were penalty based and there was no indication of excessive nodal penetrations during any of the simulations conducted. Values for the static and dynamic coefficients of friction were specified as 0.40 and 0.30 respectively.

Application of boundary conditions

The axial crushing process of the extrusion specimens was modeled by prescribing a constant velocity of 2 m/s to the rigid plate in the axial direction of the tube (negative *z*-axis direction). No other motion was permitted for the rigid plate. The bottom plate of the compressive testing machine was modeled by defining a fixed rigid wall in the *x/y* plane directly underneath the extrusion. The coefficient of friction used in the rigid wall definition was consistent with the static coefficient of friction defined in the penalty based contact definition. Nodes lying in the symmetry plane at the boundaries of the half-model were constrained to move only within the symmetry plane.

Material model

The material model used for the extrusion was required to meet a number of criteria. Due to the hardening properties observed in the tensile testing of the extrusion materials, it was necessary for the model to support non-linear plasticity. Furthermore, due to the occurrence of extrusion fracture during experimental testing, appropriate modeling of material failure was necessary.

Hanssen et al. [11] used material model 104 in LS-DYNA to predict ductile failure during the axial crushing of square tubes. This model uses the von-Mises yield criterion and incorporates non-linear plasticity. Failure is modeled using a damage mechanics theory developed by Lemaitre [12]. The model employs an effective stress, σ_{eff}, which is defined in equation (1), where D is the damage variable.

$$\sigma_{eff} = \frac{\sigma}{1-D} \qquad (0 \le D < 1) \qquad (1)$$

Lemaitre describe the effective stress as accounting for the fact that the evolution of microcracks and microcavities that occurs during inelastic loading causes a higher stress on the parts of the

material that remain undamaged. The criterion for complete rupture is given by $D = D_c$, where D_c is the critical damage value which depends on the material and loading conditions. Below the damage threshold, or the plastic strain, ε_p, at which microcracking first occurs (ε_{pD}), D remains zero. The value ε_{pD} used in these investigations was specified as 0.

Material model 104 requires for input material hardening and damage parameters ε_{pD}, D_c, and S the later thought to be a material parameter. Hanssen et al. [11] used a process of inverse modeling of tensile test specimens in order to determine these parameters and calibrate the model. This involved an iterative process of comparing the results of numerically simulated tensile tests to those of experimental tensile tests. The damage constants were altered in the models used for each iteration until the numerically determined stress versus strain curve matched the experimentally determined curve closely. It was also noted in reference [11] that the values of S and D_c are partially dependant on mesh density. Therefore, calibration of the material model is necessary to find the proper values of S and D_c.

Material model 105 in LS-DYNA was used in the present study. This material model is identical to material model 104 except that direct input of the true stress/effective plastic strain response can be incorporated into the material model. The values of S and D_c, found to be 2 MPa and 0.53 respectively, were calibrated and determined to have the best simulation prediction to the experimental observations.

Simulation procedure

All simulations were completed using LS-DYNA version 970 revision 5434a on personal computers with dual AMD Opteron 285 processors with 12 GBytes of RAM. The simulation time for each numerical simulation was approximately 8 hours.

Observations and Discussion

The load/displacement profiles from the numerical simulation and experimental results are presented in Figure 3. The five load/displacement profiles observed from the experimental tests illustrated excellent repeatability and for clarity only a single representative load/displacement profile from the experimental tests is presented in Figure 3. Predictions from the numerical simulation are in good agreement to the experimental observations up to approximately 13 mm crosshead displacement. Peak crushing loads from the experimental and numerical studies were observed to be approximately 110 kN and 120 kN respectively. In both instances, the maximum load occurred at the approximate time when the discontinuity became non-circular. In both testing methods flaring of the side wall of the extrusion at the stress concentration was observed. As the discontinuity collapsed, the crushing load decreased, and continued to do so until the complete closure of the discontinuity.

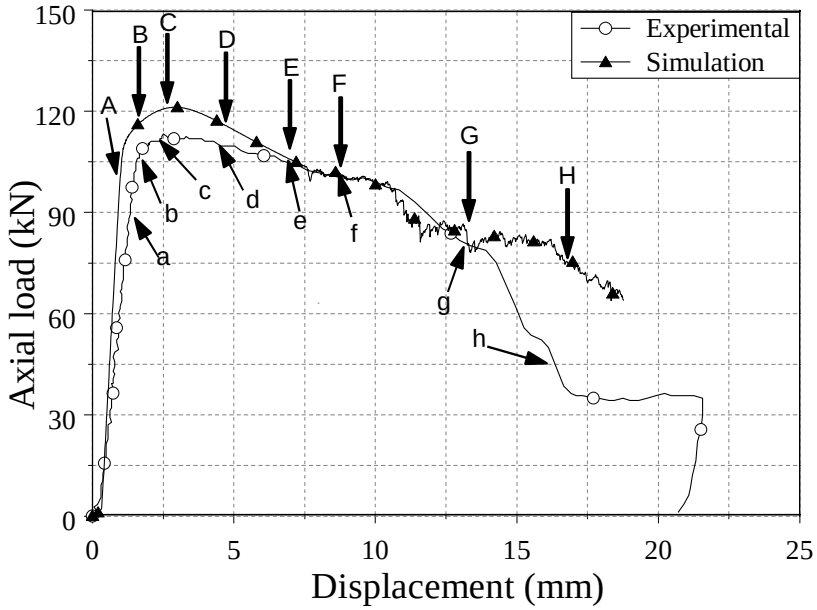

Figure 3. Load/displacement observations from numerical and experimental testing methods.

Experimental strain results are obtained through measuring the relative movement of the painted speckle pattern on the extrusion surface. As a result of the discontinuous speckled pattern near the circular hole, determination of experimental strains are slightly limited in close proximity to the edge of the hole. Additionally, as the discontinuity collapsed during crushing, the extrusion sidewall interfered with the speckled pattern to a minor extent, thus making experimental strain measurements difficult near these regions.

Fringe plots illustrating the effective strain profile near the vicinity of the discontinuity from both experimental and numerical tests are presented in Figure 4. Stages a through h and A through H correspond to the positions illustrated on the load/displacement profile presented in Figure 3. Lower case letters (a through h) correspond to the experimental observations and capitalized letters (A through H) correspond to the numerical predictions. In post-processing of the numerical simulations, the effective strains were based upon the infinitesimal strains and were in good agreement to the effective plastic strains after significantly plasticity was observed. The maximum effective strains predicted by numerical simulation were observed to be slightly larger than experimental findings. This is a result of the surface strain measurements taken by the ARAMIS system on the extrusion sidewall. For the configuration used in this investigation the ARAMIS system was unable to determine the maximum effective strain observed which is located at the mid-plane of the extrusion sidewall on either side of the discontinuity. Strain fringes, presented in Figure 4, are displayed in grayscale with an identical number of ranges set for both experimental and numerical observations. Although the identical gray shade could not be utilized in presentation of both experimental and numerical observations, the isofringe lines do correspond to identical contours of strain.

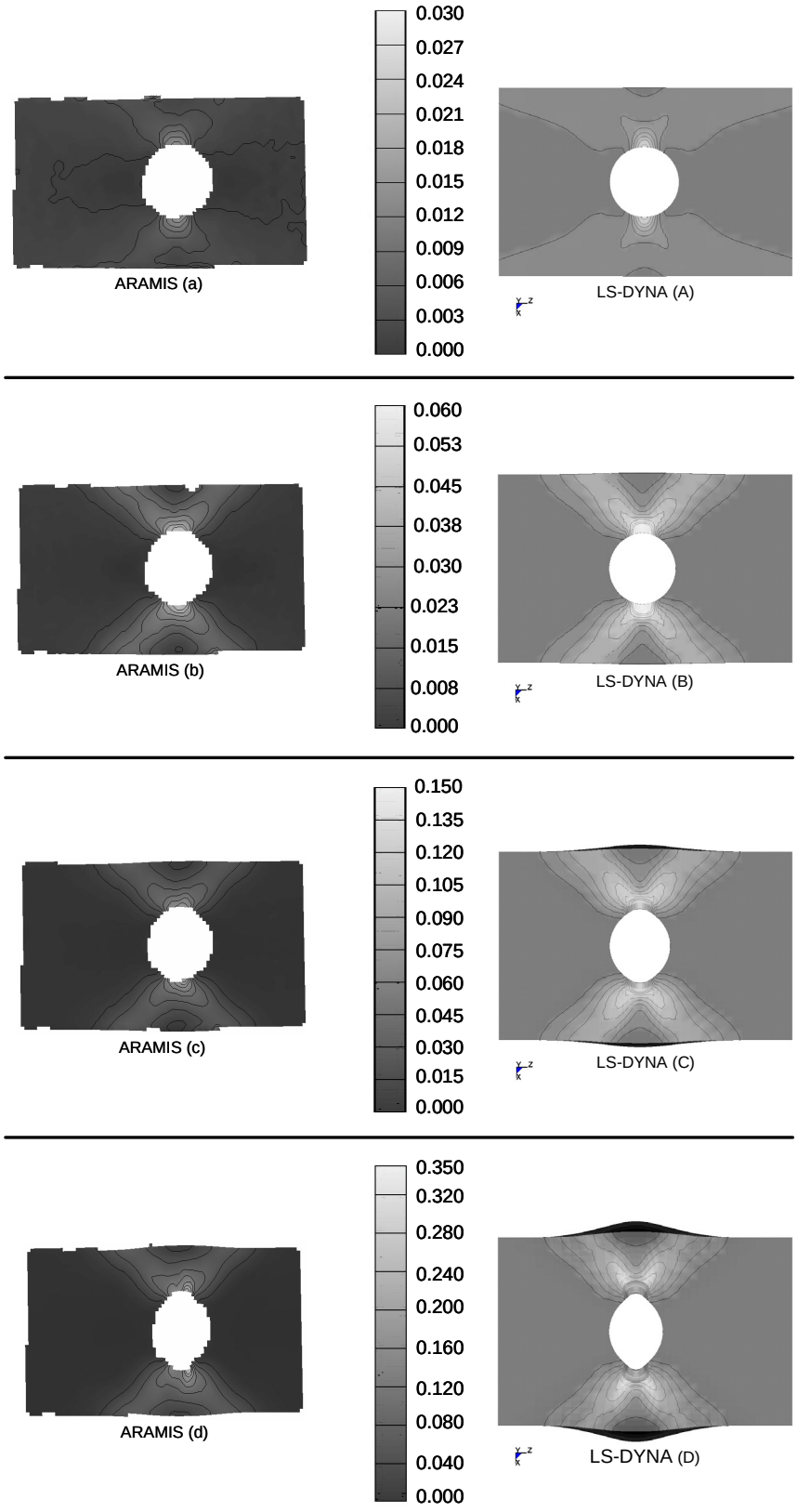

Figure 4. Comparison of LS-DYNA and ARAMIS effective strain fringe plots at various points along the load/displacement curve.

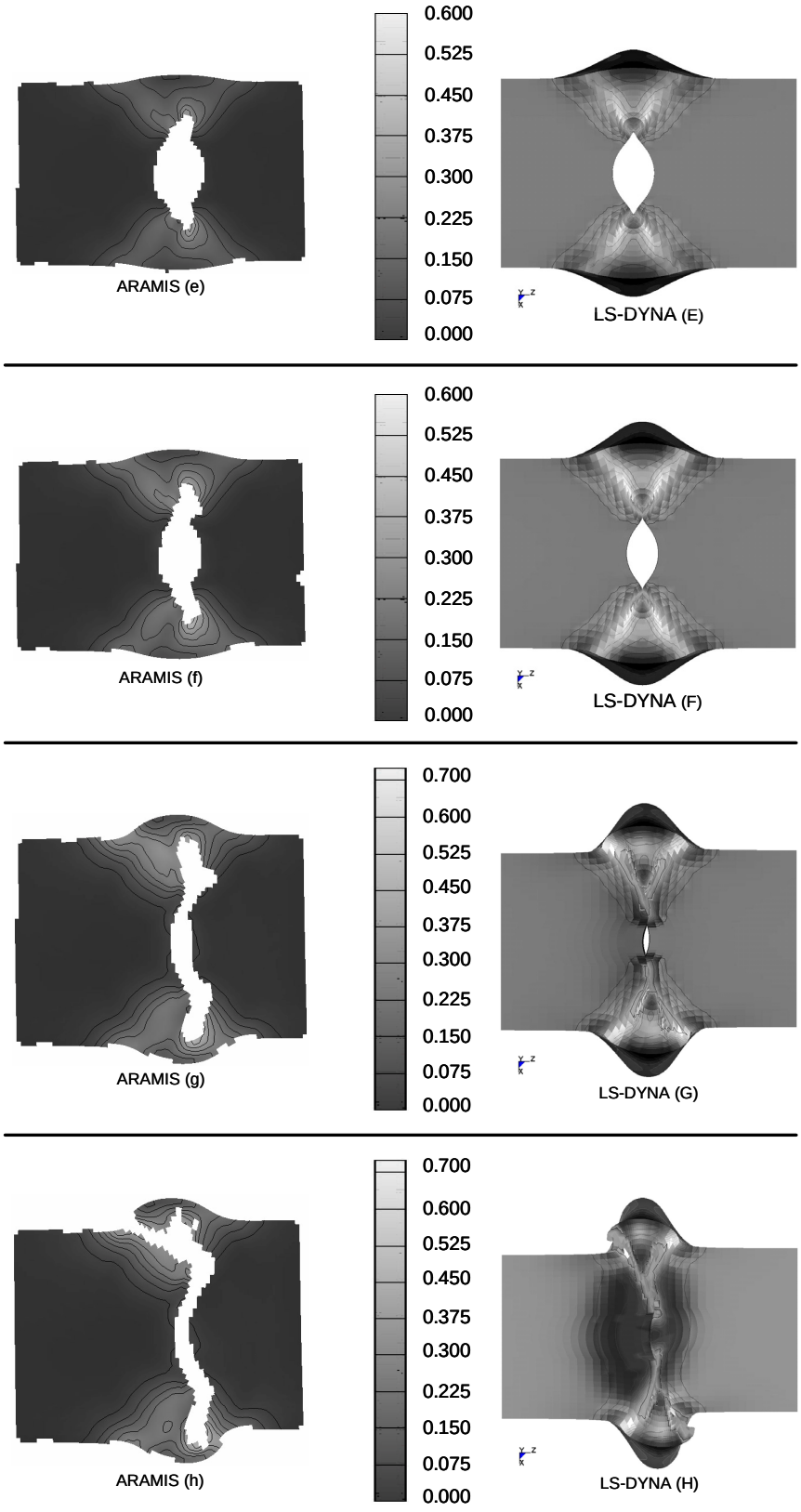

Figure 4 - continued. Comparison of LS-DYNA and ARAMIS effective strain fringe plots at various points along the load/displacement curve.

In both experimental and numerical findings, pairs of shear planes were observed to occur during crushing at angles from the centerline of the discontinuity. These planes develop early during crushing, and are clearly defined before maximum load is obtained. As the discontinuity closes, the amount of shear in the planes increases drastically. By the instant the discontinuity has completely closed, strains on the order of 70% are observed on both sides of the discontinuity. Material failure, in both experimental and numerical testing methods, occurred on the shear plane. Ductile material failure was observed to initiate at the closed (side) region of the discontinuity and propagate towards the tube side wall on the shear plane. Lack of symmetry in the experimental testing, most likely as a result of slight variations in the position of the discontinuity from the ideal centre location, resulted in failure on only one shear plane. Symmetry in numerical simulations resulted in a greater degree of material failure occurring on the other shear plane. Observations from numerical simulations indicated symmetrical material failure throughout most of the simulation, with asymmetry only arising towards the end of the analysis. It is believed that this asymmetry is a result of numerical round-off error.

Effective plastic strains on the order of 15% were observed when closing of the discontinuity commenced. Application of other material models, without appropriate material failure description would potentially implement material failure based upon the approximate 15% strain to failure from tensile testing observations. As shown in Figure 4, strains within the extrusion were in excess of 15%, which would not be achieved if other material models were used.

Conclusions

1. Validation of the ARAMIS system was completed with a series of tensile tests performed on AA6061-T6 specimens extracted from aluminum extrusions. Measurement variations between the extensometer and ARAMIS system indicated percentage errors no greater than 7%.

2. Strains predicted by LS-DYNA in the numerical simulation of the crushing process of the extrusion with a centrally located discontinuity reached values as high as 70% with significant strain concentrations observed between the sidewalls and discontinuity. Material failure was observed to occur on shear planes in both experimental and numerical testing methods.

References

[1] Jones, N. and Abramowicz, W., ‘Static and dynamic axial crushing of circular and square tubes’, Metal Forming and Impact Mechanics, Oxford, Pergamon, 1985 pp. 225–247.

[2] Abramowicz, W. and Jones, N., ‘Transition from initial global bending to progressive buckling of tubes loaded statically and dynamically’. Int J Impact Eng 1997, 19(5–6) pp. 415–37.

[3] Krauss, C.A. and Laananen, D.H., ‘A parametric study of crush initiators for a thin-walled tube’, Int J Vehicle Des 1994; 15(3–5) pp. 385–401.

[4] Abah, L., Limam, A. and Dejeammes, M., ‘Effects of cutouts on static and dynamic behaviour of square aluminum extrusions’, Fifth International Conference on Structures Under Shock and Impact, Greece, June 24–26, 1998 pp. 122–31.

[5] Arnold, B., and Altenhof, W., 'Experimental observations on the crush characteristics of AA6061 T4 and T6 structural square tubes with and without circular discontinuities', Int J Crashworthiness, 2004 9 (1) pp. 829–854.

[6] Tyson, J., Schmidt, T. And Galanilis, K., 'Biomechanics Deformation and Strain Measurements with 3D Image Correlation Photogrammetry, experimental techniques, Biomechanics Series: Part 3', 2002 September/October, pp.39-42

[7] Tyson, J., Schmidt, T., Galanulis, K., 'Advanced Photogrammetry for Robust Deformation and Strain Measurement', Proceedings of SEM 2002 Annual Conference, 2002 Milwaukee, WI, June. (www. trilion.com/pd_ARAMIS.htm)

[8] Jin, H., Lu, W. Y. and Scheffel, S., 'Full-field characterization of mechanical behavior of polyurethane foams'. International Journal of Solids and Structures, 2007 44, 6930–6944

[9] ASTM International, Standard E8M, Annual Book of ASTM Standards, Section 3, 2002, Vol. 3.01, pp.60-81.

[10] Arnold, B., 'Crush Characteristics of Quasi-Statically Loaded Square Aluminum Tubes with Circular Hole Discontinuities', M.A.Sc. thesis, Department of Mechanical, Automotive and Materials Engineering, University of Windsor, Windsor, Ontario, 2003.

[11] Hanssen, A., Hopperstad, O., Langseth, M., and Ilstad, H., 'Validation of constitutive models applicable to aluminum foams', International Journal of Mechanical Sciences, 2001, 44, pp. 359-406.

[12] Lemaitre, J., 'A course on damage mechanics', *Springer*, 1992.